Enhanced Reduction of Bromate in Water by 2-Dimensional Porous Co_3O_4 via Catalytic Hydrogenation

Duong Dinh Tuan[a], Hongta Yang[b], Nguyen Nhat Huy[c], Eilhann Kwon[d], Ta Cong Khiem [a], Siming You[e] , Jechan Lee[f,], and Kun-Yi Andrew Lin[a,*]*

[a]Department of Environmental Engineering & Innovation and Development Center of Sustainable Agriculture, National Chung Hsing University, 250 Kuo-Kuang Road, Taichung, Taiwan

[b]Department of Chemical Engineering, National Chung Hsing University, 250 Kuo-Kuang Road, Taichung, Taiwan

[c]Faculty of Environment and Natural Resources, Ho Chi Minh City University of Technology, VNU-HCM, 268 Ly Thuong Kiet St., Dist. 10, Ho Chi Minh City, Vietnam

[d]Department of Environment and Energy, Sejong University, 209 Neungdong-ro, Gunja-dong, Gwangjin-gu, Seoul, Republic of Korea

[e]James Watt School of Engineering, University of Glasgow, Glasgow G12 8QQ, UK

[f]Department of Environmental and Safety Engineering, Ajou University, Suwon 16499, Republic of Korea

*Corresponding Authors. E-mail addresses:linky@nchu.edu.tw (K. Lin); jlee83@ajou.ac.kr (J. Lee)

Abstract

As catalytic hydrogenation is validated as one of the most useful approach to reduce a potential carcinogenic bromate in water, the usage of continuous purge H_2 gas and precious metal catalysts are typically required, making it less feasible for practical implementation. Since sodium borohydride ($NaBH_4$) represents a potential alternative source for releasing H_2 and non-precious metal catalysts (cobalt (Co)) are usually required to accelerate the hydrolysis of $NaBH_4$ for faster H_2 production, the combination between Co-based catalysts and $NaBH_4$ could be favorable for bromate hydrogenation. Especially, it is even more advantageous to fabricate a porous heterogeneous catalyst with high surface area. Thus, this study aims to construct such a novel porous heterogeneous catalyst for reducing bromate using sodium borohydride. Herein, a Co-coordinated framework with TMC ligand (CoTMC) is employed as precursor, which is then transformed into hexagonal porous Co_3O_4 (HPCO) via one-step calcination. The resultant HPCO possesses remarkable surficial oxygen vacancies as well as textural properties in comparison with Co_3O_4 NP. Importantly, HPCO could completely reduce bromate to bromide within 20 min. The calculated bromate removal capacity using HPCO and $NaBH_4$ is achieved as 781.25 μmol/g, and the activation energy (E_a) is also calculated as 28.5 kJ/mol. Besides, HPCO also exhibits high catalytic activities for bromate reduction in the presence of various anions. Moreover, HPCO could be also reusable for reducing bromate to bromide over multiple-cycles without any remarkable change of catalytic activities. These features indicate that HPCO is a robust and effective heterogeneous catalyst for bromate reduction in water.

Keywords: hydrogenation, bromate, bromide, H_2, cobalt, Co_3O_4,

1. Introduction

Bromate anion (BrO_3^-), a typical bromine-based oxidation product, has been commonly found in different water systems [1, 2]. Since bromate is regarded as a potential human carcinogenic compound, its maximum concentration has been regulated at 10 μg/L by WHO and USEPA [3]. While the formation of bromate from ozonation process was reported previously [4], some recent studies also illustrated that bromate can be formulated via advanced oxidation processes (AOPs) [5, 6]. Since AOPs have been extensively employed for wastewater treatments, it is critically urgent to remove bromate in water.

To date, there are numerous approaches for removing bromate including filtration [7], adsorption [8], biodegradation [9] and catalytic reduction [6, 10-16]. Nevertheless, bromate is ineffectively removed via traditional techniques (e.g., filtration, adsorption or biodegradation) due to high-cost, long operation time and low bromate removal capacities. On the contrary, catalytic reduction stands out as a promising approach, in which bromate can be removed and converted expeditiously to bromide ions in the presence of reducing agents (e.g., H_2 gas) [10, 12, 16].

Recently, since the usage of continuous purge H_2 usually suffers from difficulties of low solubility, safety concerns and sophisticated storage, chemical hydrides (e.g., NH_3BH_3, $LiBH_4$, $NaBH_4$), in particular, sodium borohydride ($NaBH_4$) receives increasing attention as a potential reductant to replace conventional H_2 gas to reduce bromate in water because $NaBH_4$ possesses high theoretical H_2 capacity (*ca.* 10.8 wt%), easy-handling and environmental friendliness [6, 11, 17-19]. Nevertheless, the self-decomposition of $NaBH_4$ in water for releasing H_2 gas is significantly low, making it inefficient to quickly reduce bromate ions. Thus, catalysts are usually required as an "activator" to facilitate H_2 released from $NaBH_4$ hydrolysis [20]. For instance, Nurbek and co-workers employed a Ni-based MOF for catalyzing $NaBH_4$ to reduce bromate to

bromide [21]. Lin et al. prepared nanoscale cobalt/carbon nanocage (NCC) to facilitate hydrolysis of $NaBH_4$ to quickly release H_2 to convert bromate to bromide [6]. Another previous work also investigated MOFs as catalysts for accelerating $NaBH_4$ hydrolysis to reduce bromate in water [22].

Recently, precious metal catalysts have been investigated and exhibited high catalytic activities to bromate reduction [12, 23, 24]; however their expensiveness and scarcity restrict them for large-scale applications. In contrast, non-precious metal catalysts have been validated as potential alternatives implemented for removing bromate in water [6, 11, 12, 21, 25-27]. In particular, cobalt (Co) is proven as one of the most effective non-precious metal catalysts employed for catalyzing $NaBH_4$ hydrolysis and eliminating toxicants in water [6, 25, 28]. While homogeneous Co-based catalysts are commonly inconveniently employed for practical applications, heterogeneous Co-based catalysts, in particular, cobalt oxide (Co_3O_4) has been recently attracted increasing attention and extensively used for various catalytic applications [28-32]. Nonetheless, as bromate reduction is conducted in aqueous environment, Co_3O_4 nanoparticles (NPs) are easily accumulated in aqueous solution, hence losing its catalytic activities [33, 34].

In this regard, immobilized/supported Co_3O_4 NP composites are validated as promising approaches to minimize aggregation issue [32, 35], however sophisticated procedure and long fabrication time are typically required, making it less feasible for practical applications. On the contrary, Co_3O_4 catalysts derived from Cobalt-based precursor could be another strategy, in which Co_3O_4 NP can be completely framed, therefore those NPs might be avoided from agglomeration [28, 29]. More importantly, the fabricated Co_3O_4 catalyst could not only retain the morphology of the precursor but also consist of pores, enabling it become a porous Co_3O_4 catalyst [29, 36]. This porous-structured Co_3O_4 catalyst should be advantageous for hydrolyzing $NaBH_4$ for H_2 production, then reducing bromate in water.

Herein, in this study, we proposed developing a robust and effective Co_3O_4 through a single step calcination of a Co-coordinated framework with TMC ligand (CoTMC), which was then employed for eliminating and reducing bromate in water. The resultant material not only retained the 2-dimensional (sheet-like) hexagonal morphology of CoTMC but also exhibited porosity, making it a hexagonal porous Co_3O_4 (HPCO). Unique characteristics of the as-prepared HPCO were analyzed by Scanning Electronic Microscopy (SEM), Transmission Electron Microscopy (TEM), X-ray powder diffraction (XRD), X-ray photoelectron spectroscopy (XPS), Raman spectroscopy. Besides, the effect of different parameters including catalyst and $NaBH_4$ concentrations, pH, temperature, co-existing anions using HPCO+$NaBH_4$ for bromate reduction is also investigated. The reusability of HPCO was also evaluated and the catalytic reduction mechanism of bromate by HPCO+$NaBH_4$ system was also interpreted.

2. Experimental

2.1 Materials

All chemicals reagents in this study were purchased from commercial suppliers and used as received without further purifications. Cobalt chloride ($CoCl_2$) (>98%) was obtained from Choneye Pure Chemicals (Taiwan). Trismercaptotriazine (TMC) ($C_3H_3N_3S_3$) (95%) was purchased from Alfa Aesar (USA). Sodium borohydride ($NaBH_4$) (>98%) was received from Acros Orgabics (USA). (Deionized (DI) water was prepared to less than 18 MΩ-cm.

2.2 Preparation and characterization of HPCO

The fabrication procedure of HPCO was illustrated in Fig. 1(a). Firstly, the coordinated framework comprised of Co and TMC (CoTMC) was prepared by coordinating Co^{2+} ions with TMC ligand [37]. In brief, 0.015 mol of $CoCl_2$ was dissolved in 200 mL of DI water, followed by the addition of 0.017 mol of TMC. The mixture was then continuously stirred at ambient temperature for 1 h, then aged without stirring for 24 h. The precipitate was collected by centrifugation, washed thoroughly by DI water/ethanol and dried at 65^{o}C to afford CoTMC. Subsequently, CoTMC was calcined in air at 550^{o}C to result in HPCO.

Morphologies of HPCO were visualized using electronic microscopies (JEOL JSM-7800F and JEM-1400, Japan). The crystalline structure of HPCO was then analyzed by an X-ray diffractometer (Bruker, USA). The chemical composition was also determined by EDX spectroscopy (Oxford Instruments, UK). Moreover, the surface chemistry of HPCO was further examined by X-ray photoelectron spectroscopy (PHI 5000, ULVAC-PHI, Japan). The textural properties of HPCO were analyzed by a volumetric analyzer (Anton Paar ASIQ, Austria) to obtain the N_2 sorption isotherms. Temperature-programmed reduction (TPR) profiles of catalysts were determined by a chemisorption analyzer with a TCD detector (Anton Paar, ASIQ TPx, Austria). Raman spectroscopies of HPCO and commercial Co_3O_4 NP were determined using a Raman spectrometer (TII Nanofinder 30, Japan). Zeta potentials of HPCO were analyzed by a zetasizer (Malvern, UK).

2.3 Catalytic reduction of bromate

The catalytic activity of HPCO for bromate reduction was performed using batch experiments. In a typical experiment, a certain amount of HPCO (e.g., 100 mg/L) was added to 200 mL of bromate solution with the initial bromate concentration (C_0) was 10 mg/L (equivalent to 0.78 mM). At a certain reaction time *t*, a sample aliquot was withdrawn from the mixture and filtered by syringe filter (0.22 μm). Subsequently, the filtrate was analyzed using an ion chromatography system (Dionex ICS-1100, USA) to determine concentrations of residual bromate (C_t) and generated bromide (C_j) at a given time *t*. The bromate removal efficiency (q_t) of HPCO was calculated via the following formula (Eq. (1)):

$$q_t = \frac{(C_0 - C_t) \times V}{W} \qquad (1)$$

where *V* is the solution volume and *W* is the mass of the catalyst. The generation capacity of bromide from reduction of bromate (q_j, μmol/g) at a certain reaction time was measured via the following formula (Eq. (2)):

$$q_j = \frac{(C_j - C_i) \times V}{W} \qquad (2)$$

where C_j is the concentration of bromide detected in the solution at a certain time t; and C_i is the initial concentration of bromide in the solution. The effect of different pH parameters (i.e., 3-11) was evaluated by adjusting the initial pH bromate solution using HCl (1M) and NaOH (1M). The effect of co-existing anions (e.g., nitrate, sulfate, phosphate) was examined by adding the equivalent concentration (i.e., 10 mg/L) to bromate solution. Recyclability of HPCO was performed by reusing recovered HPCO without any regeneration treatments.

3. Results and discussion

3.1 Characterizations of HPCO

Firstly, morphologies of the pristine precursor CoTMC were characterized to probe its appearance. Fig. 1(b) and (c) present SEM and TEM images of the as-fabricated CoTMC, showing that CoTMC possessed a hexagonal sheet-like morphology with smooth surfaces. After calcination processes, the resultant product still retained the hexagonal nanosheet-like morphology (shown in Fig. 1(d)) with the appearance of many pores. TEM image in Fig. 1(e) further reveals that those pores certainly existed and distributed throughout the substrate, confirming that the resultant calcined product was converted into a porous hexagonal nanosheet material. Moreover, Fig. 1(f) also reveals that this calcined material was not only porous but also comprised of various spherical nanoparticles (NPs). The lattice-resolved HRTEM of this material showed two particular *d*-spacing values of 0.244 and 0.220 nm (Fig. 1(g)), which could be ascribed to the crystal plane of (311) and (220) of Co_3O_4, respectively. This result confirms that the above-mentioned spherical NPs should be attributed to Co_3O_4, demonstrating that CoTMC had been successfully transformed to Co_3O_4 after the calcination process, creating porous hexagonal nanosheet Co_3O_4 (HPCO). The inset of Fig. 1(g) provides the SAED of HPCO, illustrating a poly-crystalline structure of HPCO [38, 39]. Besides, the size of those Co_3O_4 NPs HPCO was also determined in Fig. S1, confirming the nanoscale dimensions of these NPs.

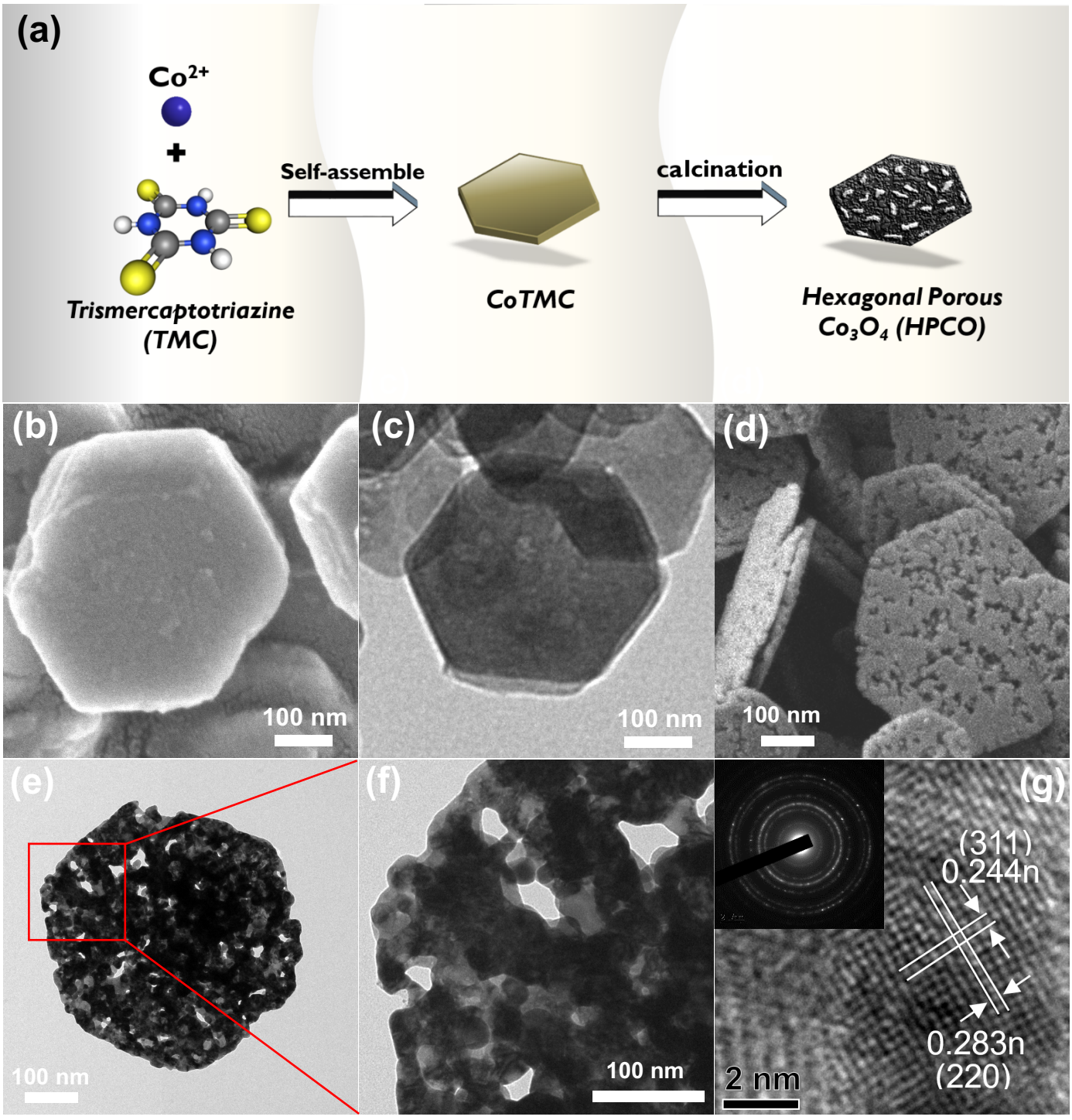

Fig. 1. (a) Schematic illustration for preparing HPCO; (b) SEM and (c) TEM images of CoTMC; (d) SEM and (e) TEM images of HPCO; and (f), (g) HRTEM images of HPCO (the inset is the SAED of HPCO).

The elemental analysis of HPCO was also determined using EDX spectroscopy as shown in Fig. 2(a) in which noticeable signals of Co and O were detected. A small peak at 0.3KeV could be ascribed to carbon (C), which possibly derived from carbon-coated layer on specimens. Besides, the crystalline structures of the pristine CoTMC and the resultant HPCO were further analyzed. Since the XRD patterns of CoTMC exhibited several noticeable peaks at 19, 32, 38, 51, 58, 61.6, 69.6 and 71.4° (Fig. S2), which were well-indexed to reported patterns [37], the resulting HPCO showed totally different XRD patterns. Particularly, several diffraction peaks at 19.0°, 31.3°, 36.8°, 38.5°, 44.8°, 59.4° and 65.2° could be detected as shown in Fig. 2(b), which were corresponded to Co_3O_4 according to JCPDS #42-1467, further asserting the formation of Co_3O_4 of HPCO.

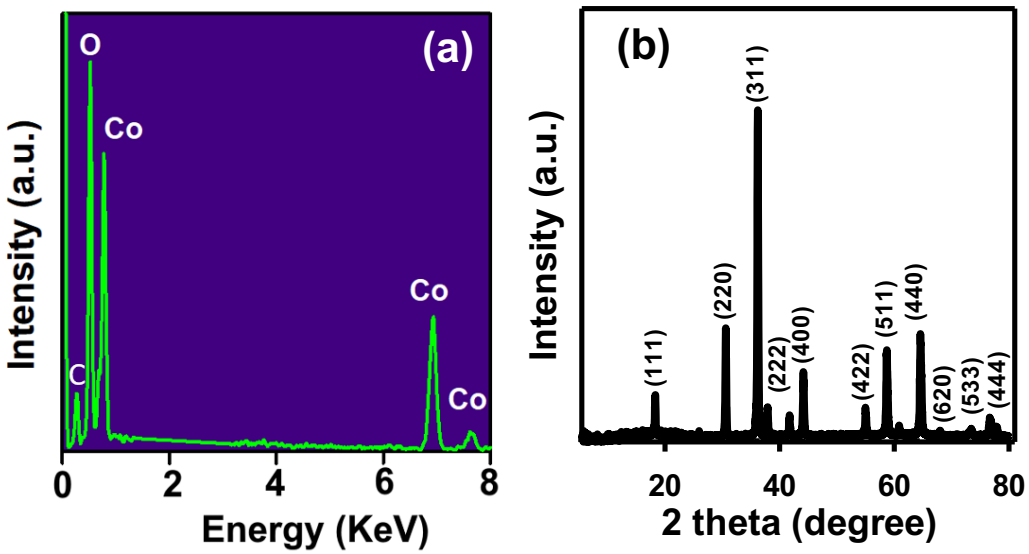

Fig. 2. Characterizations of HPCO: (a) EDX, and (b) XRD

Additionally, an IR spectrum of HPCO was presented in Fig. 3(a). Two noticeable peaks could be observed at 565 and 660 cm^{-1}, corresponding to the stretching vibration modes of cobalt oxide for the tetrahedrally-bound Co^{2+} as well as octahedrally-bound Co^{3+}, respectively [40]. This result confirms the nature co-existence of Co^{2+} and Co^{3+} species in Co_3O_4. Moreover, some small peaks

were also detected at 1630 and 3350 cm^{-1}, attributed to the stretching and bending modes of (OH), which possibly derived from water molecules adsorbed on HPCO surfaces [41]. Furthermore, Raman spectroscopic analysis of HPCO was performed in Fig. 3(b), and some noticeable peaks could be found at 190, 472, 515 and 678 cm^{-1}, corresponded to F^1_{2g}, Eg, F^2_{2g} and A_{1g} modes of Co_3O_4, respectively [42]. As Raman spectroscopy is commonly employed to verify oxygen vacancies of metal oxides, the reference catalyst, commercial Co_3O_4 NP, was also analyzed and compared with HPCO to probe differences of oxygen vacancies between HPCO and the commercial Co_3O_4 NP. As shown in Fig. 3(b), Raman spectrum of Co_3O_4 NP was comparable to that of HPCO, indicating that no obvious disordered structure of Co_3O_4 was present in HPCO [43]. Nevertheless, a closer spectra comparison between two materials at F^1_{2g} and A_{1g} modes (displayed in Fig. 3(c) and (d)) reveals that these peaks had shifted. Particularly, the peak of F^1_{2g} shifted from 190 to 193 cm^{-1}, while the peak of A_{1g} changed from 677 to 685 cm^{-1}. Since these peaks of F^1_{2g} and A_{1g} were associated with Co^{2+}-O^{2-}, and Co^{3+}-O^{2-}, respectively [44, 45], these shifting indicated that HPCO showed a higher degree of surficial oxygen vacancies than Co_3O_4 NP [46].

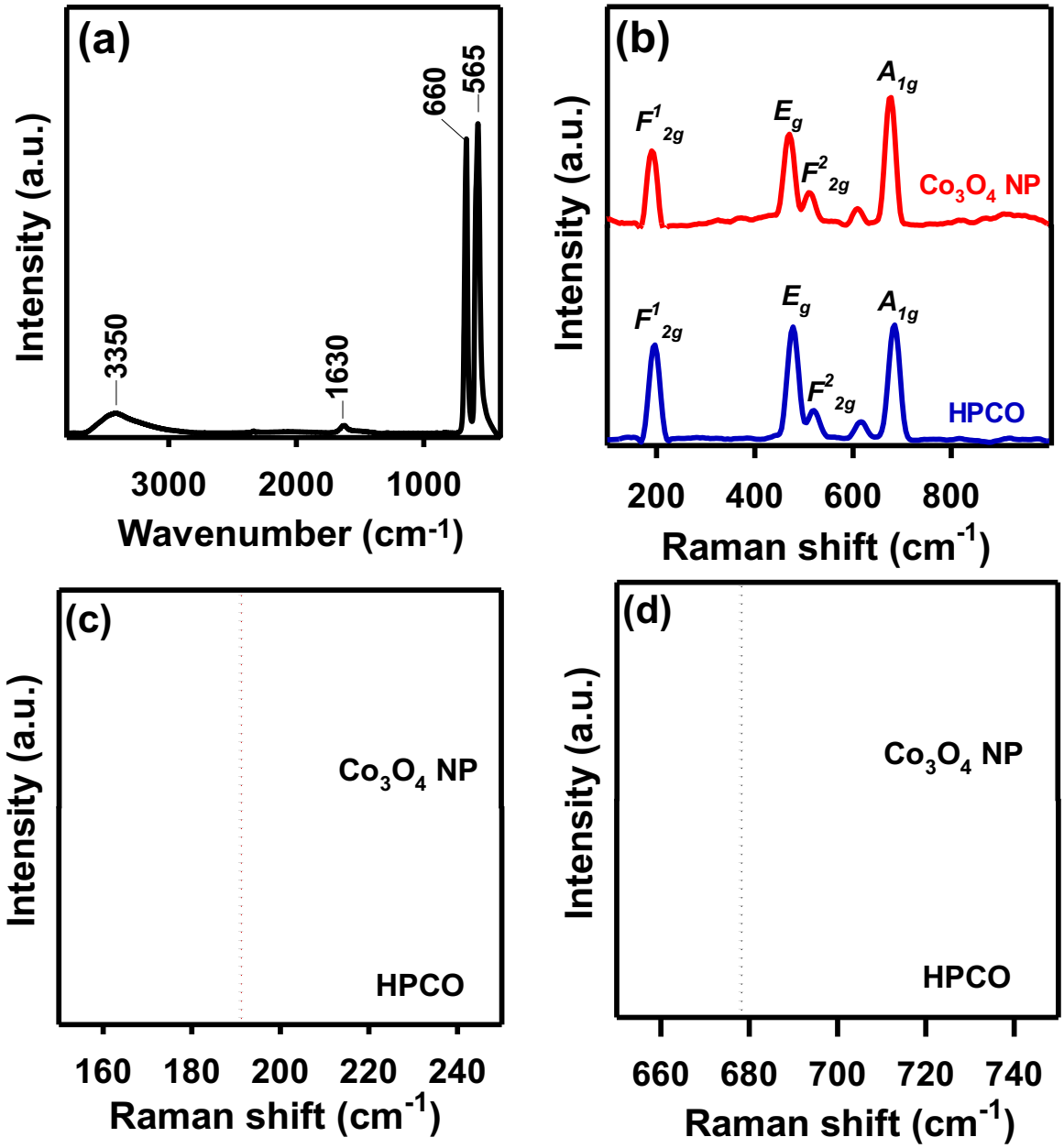

Fig. 3. Spectroscopies analyses of HPCO: (a) FTIR, (b) long-range Raman spectroscopy, (c) and (d) short-range Raman spectra at the regions of F^1_{2g} *and* A_{1g}.

Furthermore, the surface chemistry of HPCO was also analyzed using XPS analysis. A full-survey spectrum of HPCO (Fig. S3) was determined, showing only Co and O species were detected. Fig. 4(a) also presents the Co2p spectrum of HPCO, which could be deconvoluted into multiple peaks. Particularly, the peaks at 779.2 and 794.1 eV could be corresponded to Co^{3+} species whereas

the peaks at 780.6 and 795.8 eV could be ascribed to Co^{2+} species. These detected Co species further assures that the presence of Co_3O_4 in HPCO [47]. Besides, the O1s spectrum of HPCO was also analyzed as shown in Fig. 4(b), and two noticeable peaks at 529 and 531 eV could be attributed to metal-oxygen bond and R-O bond, respectively [48].

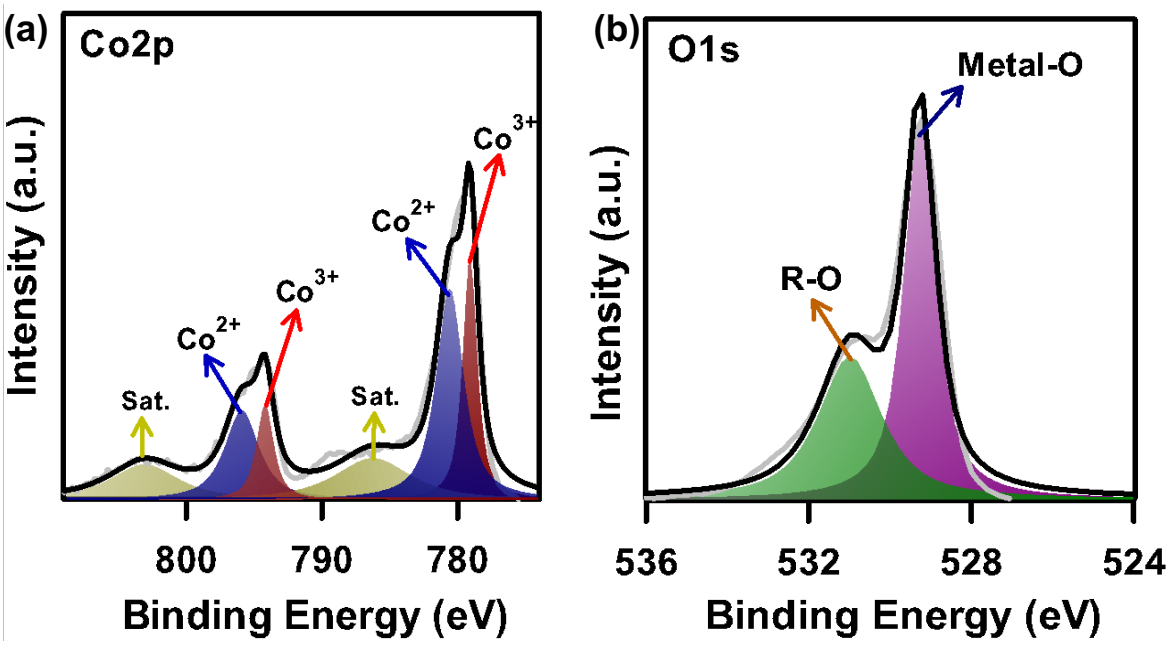

Fig. 4. XPS analysis of HPCO: (a) Co2p, and (b) O1s core-level spectra.

To further elucidate differences between HPCO and the commercial Co_3O_4 NPs, their redox characteristics were then determined by temperature-programmed reduction (TPR) measurements. Fig. 5(a) displays TPR profiles of HPCO and the commercial Co_3O_4 NP. The reduction process of HPCO started at a relatively low temperature at ca. 250 °C, and a center temperature of the overall reduction profile occurred at 440 °C, whereas the reduction process of Co_3O_4 NP started at 350 °C with a center temperature at 475 °C. These comparisons indicated that while HPCO and the commercial Co_3O_4 NPs both consisted of Co_3O_4, their redox characteristics were noticeably different possibly owing to distinct surficial and morphological differences between these two catalysts.

In addition, textural properties of HPCO were also examined using N_2 sorption isotherms. As displayed in Fig. 5(b), the sorption isotherm of HPCO could be considered as an IUPAC type I isotherm, revealing that HPCO contained fine pores. The inset in Fig. 5(b) presented the pore size distribution, indicating that HPCO certainly comprised of mesopores, the corresponding specific surface area of HPCO was then measured as 13 m^2/g with a pore volume of 0.06 cm^3/g. For comparison, textural properties of a commercial Co_3O_4 NP were also characterized as shown in Fig. S4, and its specific surface area was determined as 2 m^2/g with a pore volume of 0.01 cm^3/g. This result demonstrates that HPCO possessed superior textural properties in comparison with that of Co_3O_4 NP, probably because Co_3O_4 NPs are easily agglomerated (as shown in Fig. S4)). On the contrary, though HPCO was also comprised of spherical Co_3O_4 NPs, these NPs could be refrained from agglomeration since Co_3O_4 NPs were framed into the 2D morphology.

Since catalytic reduction of bromate using HPCO catalyzed $NaBH_4$ is an aqueous-solution reaction, it was necessary to determine the surface charges of HPCO under different conditions using zeta potentials analysis as shown in Fig. 5(c). One can be seen that the surface charges of HPCO became more negative as the increase of pH. In particular, at pH = 3, the surface charge of HPCO was +31mV, which was slightly reduced to +6 mV at pH = 5, then decreased to 0, -5 and -29 mV at pH = 7, 9 and 11, respectively. This result reveals that the surface charges of HPCO were positive under acidic conditions, then turned to negatively-charged under basic conditions with a pH_{zpc} = *ca*. 7.

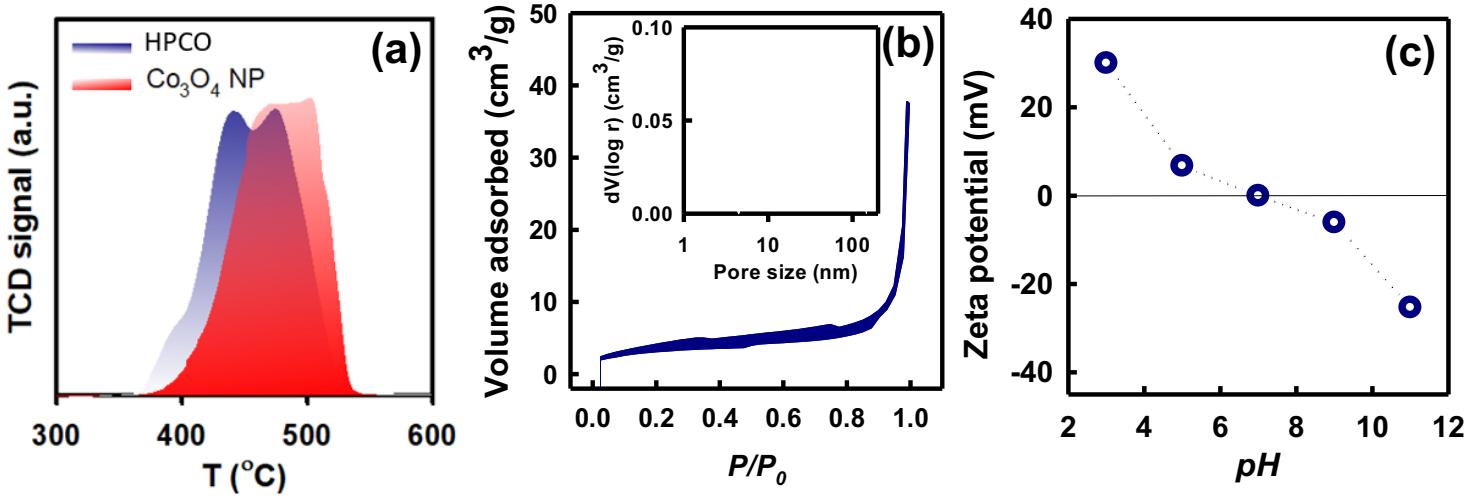

Fig. 5. Properties of HPCO: (a) TPR profile, (b) N_2 sorption isotherm and pore size distribution, and (c) zeta potentials.

3.2 Bromate reduction using HPCO with $NaBH_4$

Since bromate reduction was conducted in the presence of HPCO as an "activator" and $NaBH_4$ as a source for releasing H_2, the reduction of bromate was firstly measured using individual constituent. Fig. 6(a) shows that bromate was negligibly reduced in the presence of HPCO alone, demonstrating that HPCO itself was incapable of removing bromate. When $NaBH_4$ was individually used to reduce bromate (without addition of catalysts), the concentration of bromate was barely decreased as C_t/C_0 was only 0.94, indicating that $NaBH_4$ alone could not reduce bromate efficiently, either. Nevertheless, when HPCO and $NaBH_4$ were simultaneously present, bromate was quickly reduced as C_t/C_0 reached nearly zero after 20 min, illustrating the effectiveness of HPCO catalyzed $NaBH_4$ to reduce bromate in water. The residual bromate concentration remained in the solution after reduction process was only 0.03 μg/L, which is below the maximum bromate concentration in drinking water (i.e., 0.078 μg/L) regulated by WHO and USEPA. On the other hand, as HPCO was comprised of Co_3O_4 NP, the commercial Co_3O_4 NP was

also employed as a reference catalyst for bromate reduction. As shown in Fig. 6(a), bromate was gradually reduced using commercial Co_3O_4 NP with C_t/C_0 only reached 0.79 after 60 min, which was much higher than that of HPCO. This result further confirms the superior catalytic activities of HPCO to bromate reduction in comparison with commercial Co_3O_4 NP.

Nevertheless, since the term of Ct/C0 did not signify the amount of bromate reduced; therefore, bromate removal efficiencies per gram of catalyst (μmol/g) were necessarily determined as shown in Fig. 6(b). There was a small fraction of bromate (i.e., 44.7 μmol/g) was removed in the presence of sole $NaBH_4$ after 60 min, proving that without the addition of catalyst, bromate was inefficiently reduced. Besides, while bromate removal efficiencies (q_t) at 60 min of CoTMC and commercial Co_3O_4 NP were 101.6 and 163.9 μmol/g, respectively, HPCO exhibited a much higher bromate removal efficiency as q_t could reach nearly 781.25 μmol/g, an equilibrium, which is even higher than other reported catalysts in literature (shown in Table S1). This result further confirms that HPCO is an advantageous and promising heterogeneous catalyst for reducing bromate in water.

On the other hand, it was also crucial to determine whether bromate could be converted to bromide by those above-mentioned materials. As displayed in Fig. 6(c), almost no bromide generated after 60 min using sole $NaBH_4$. When CoTMC and the commercial Co_3O_4 NP were employed, bromide generation capacities (q_j) were certainly detected, revealing that bromate was surely reduced to bromide. Moreover, as HPCO exhibited outstanding catalytic activities to bromate elimination, the corresponding generated bromide was also significantly higher than other materials, asserting the superior catalytic activity of HPCO for reducing and converting bromate to bromide. One can be noted that the generated bromide capacities were typically comparable to the amount of bromate reduced, suggesting that bromate was predominantly converted to bromide,

and there was nearly no adsorption of removed bromate ions or produced bromide ions onto HPCO surface (Fig. S5).

As hydrolysis of $NaBH_4$ for releasing H_2 can be expedited in the presence of metal catalysts as follows (Eq.(3)) [49, 50]:

$$NaBH_4 + 2H_2O \rightarrow NaBO_2 + 2H_2 \quad (3)$$

the reaction of $NaBH_4$ with HPCO would produce H_2 which might then react with bromate to become bromide and H_2O as follows (Eq. (4)):

$$BrO_3^- + 3H_2 \rightarrow Br^- + 3H_2O \quad (4)$$

Fig. 6(d) shows H_2 evolution by $NaBH_4$ in the presence of HPCO, and H_2 evolution proceeded rapidly along with the reaction time, approaching an equilibrium after 20 min. The tendency of H_2 evolution was similar to that of bromate reduction in Fig. 6(a), suggesting that removal of bromate by HPCO+$NaBH_4$ would correlate to the reaction expressed in Eq. (4), which could take place via multiple potential mechanisms [12]. Firstly, H_2 would be evolved from HPCO-catalyzed hydrolysis of $NaBH_4$, and the resulting H_2 would react with bromate ions in the bulk phase to transform bromate to bromide as illustrated in Fig. 6(e) as the route (i). On the other hand, bromate might temporarily reside on the surface of HPCO, and contact with H_2 molecules derived from HPCO-catalyzed $NaBH_4$ to become bromide as the route (ii) in Fig. 6(e).

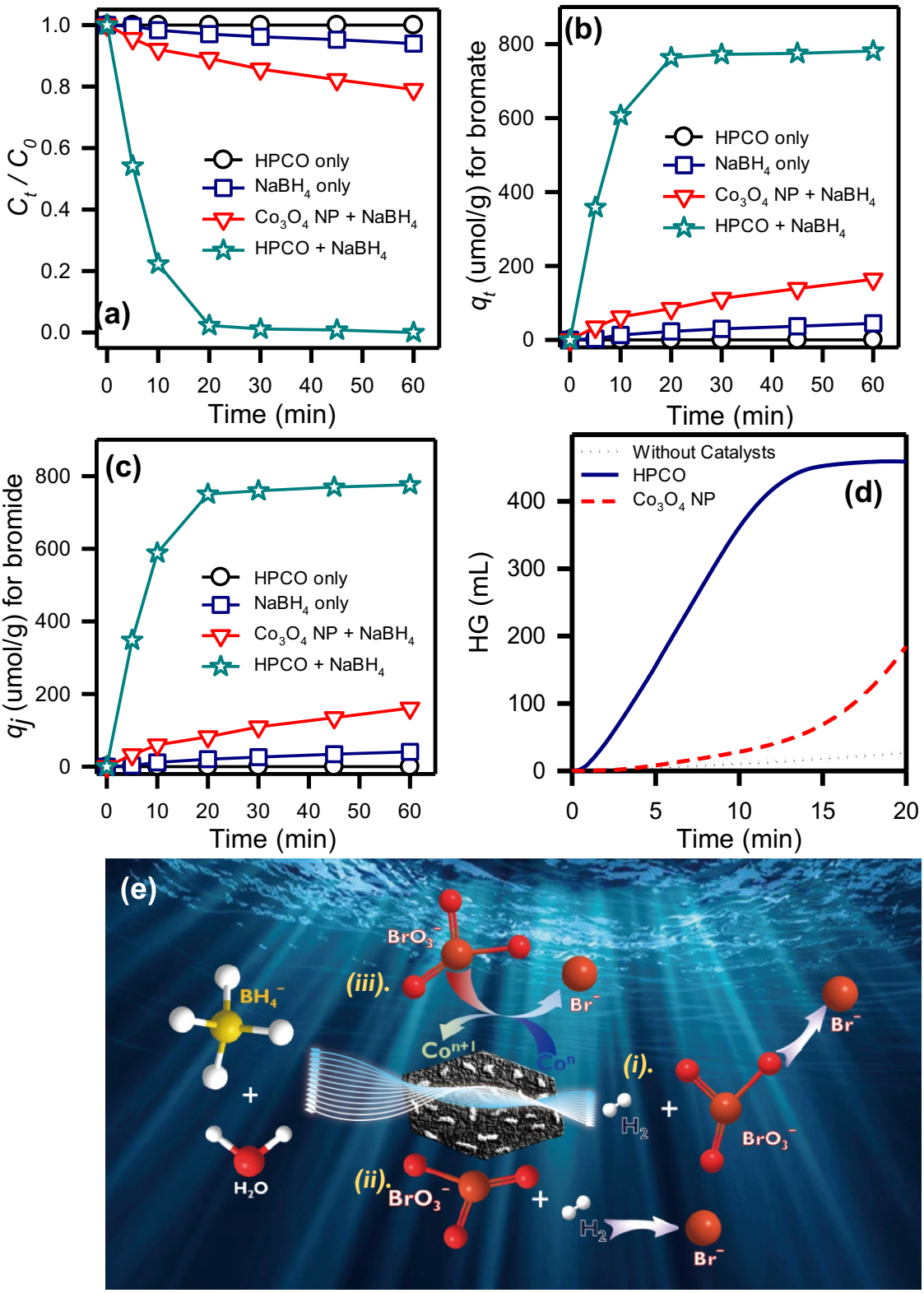

Fig. 6. Comparisons between HPCO only, $NaBH_4$ only, Co_3O_4 NP+ $NaBH_4$ and HPCO+$NaBH_4$ for (a) bromate removal in terms of Ct/C0, (b) removal efficiency for bromate, (c) conversion efficiency of bromide (catalyst = 100 mg/L, $NaBH_4$ = 100 mg/L, T = 30°C); (d) H_2 generation (T = 30°C, catalyst = 500 mg/L, and $NaBH_4$ = 125 mM); and (e) the mechanisms of bromate reduction by HPCO+NaBH4

Besides, as HPCO contained Co^{2+}, Co^{2+} would donate electrons to bromate and transform it to bromide while Co^{2+} was oxidized to Co^{3+} as the route (iii) in Fig. 6(e). Thus, XPS spectroscopy of used HPCO was analyzed as shown in Fig. S6; and the peak intensities of Co^{2+} and Co^{3+} were obviously changed compared to the pristine HPCO. This result validated that the oxidation of Co^{2+} to Co^{3+} certainly happened, which was then contributed to the reduction of bromate as illustrated in route (iii) of Fig. 6(e). Pandey et al. employed $Ti_3C_2T_x$ (MXene) for removing bromate and reported that the oxidation of Ti^{2+} to Ti^{4+} provided electrons to reduce bromate to bromide [51]. Another work by Restivo and co-workers also found that the reduction of bromate was certainly happened on the surface of metal catalyst in the presence of hydrogen atom in which metal was oxidized while bromate was contemporary reduced into bromide [12].

3.3 Effect of catalyst and $NaBH_4$ dosages

Since catalyst and $NaBH_4$ dosages are two crucial components to bromate reduction, the effect of HPCO dosage was first examined as displayed in Fig. 7(a-c). As discussed above, bromate was inefficiently removed in the absence of catalyst. Nevertheless, since a small amount of HPCO was adopted (i.e., 50 mg/L), the concentration of bromate was certainly reduced as C_t/C_0 was nearly 0.4 after 60 min with the corresponding removed bromate capacity was 1359.7 μmol/g. When HPCO dosage was increased to 100 mg/L, the concentration of bromate was quickly decreased as C_t/C_0 reached to nearly zero, and q_t was slightly reduced as 781.2 μmol/g. Further increase of HPCO dosage from 150 to 200 mg/L resulted in faster bromate reduction as C_t/C_0 could reach nearly zero in a shorter time with the corresponding q_t were 520.8 and 390.5 mg/L, respectively. These results reveal that though higher dosages of HPCO were more beneficial for reducing bromate, the removal efficiencies were decreased correspondingly. This is possibly because a

higher dosage of catalyst did not fully contribute to the reduction of bromate in water, which is similar to reported literatures [14, 52]. Moreover, one can be noted that bromide generation capacities were still comparable to reduced bromate concentrations, demonstrating that there were almost no adsorptions of bromate/bromide ions onto HPCO even at a higher dosage of HPCO.

In addition to catalyst dosage, since the presence of $NaBH_4$ as H_2 source is another important parameter for reducing bromate, it is also important to evaluate the variation of $NaBH_4$ dosage using HPCO as displayed in Fig. 7(d-f). At $NaBH_4$ = 50 mg/L, the concentration of bromate was gradually reduced as C_t/C_0 was 0.42 at 60 min, indicating that the reduction of bromate was insignificant in the lack of HG released from $NaBH_4$. Since $NaBH_4$ dosage was increased to 100 mg/L, bromate was rapidly reduced and fully removed within 20 min as C_t/C_0 reached nearly zero. Moreover, further increase of 125 mg/L of $NaBH_4$ enabled even faster bromate reduction within a certain shorter time. This finding suggests that a certain $NaBH_4$ dosage (i.e., 100 mg/L) is needed to afford completely bromate elimination by HPCO catalyzed $NaBH_4$ system. Similar results were also reported in literatures that bromate could be totally eliminated/reduced at a fixed amount of $NaBH_4$ [6]. For further experiments, 100 mg/L of $NaBH_4$ is particularly selected to investigate other parameters.

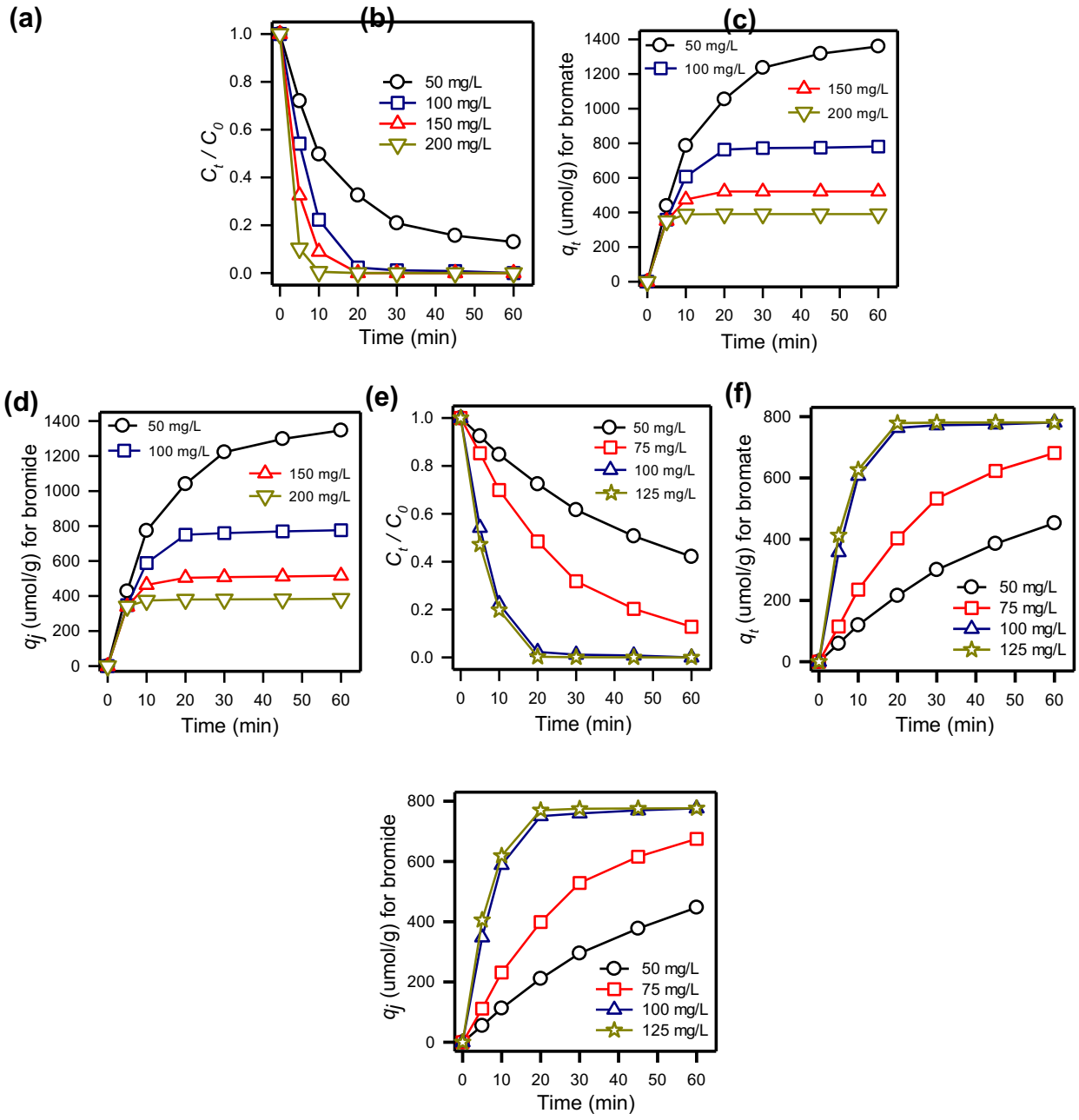

Fig. 7. Effect of catalyst (a-c) and $NaBH_4$ dosage (d-f) on bromate reduction using HPCO+$NaBH_4$ (HPCO = 100 mg/L, $NaBH_4$ = 100 mg/L, T = 30°C).

3.4 Effect of temperatures

Temperature is also a critical factor for bromate reduction in water; therefore, the effect of different temperatures varying from 30 °C to 40 °C to bromate reduction using HPCO catalyzed $NaBH_4$ was further examined. As displayed in Fig. 8, bromate was totally eliminated/reduced within 20 min at 30 °C, which was even faster in shorter time at higher temperatures. In particular, 100% of bromate was achieved in 15 min at 35 °C whereas all bromate was reduced within 10 min at 40 °C. This validates the enhancing effect of elevated temperatures on bromate reduction using HPCO/$NaBH_4$ system. Besides, bromate removal kinetics at various temperatures were further calculated via the pseudo first order rate law as the following equation (Eq. (5)):

$$C_t = C_0 \exp(-k_{obs}t) \qquad (5)$$

where k_{obs} (min^{-1}) represents the observed rate constant of the pseudo first order equation. At 30 °C, bromate reduction kinetics was calculated as 0.148 min^{-1} (Table S2), which was significant increased to 0.1758 min^{-1} and 0.213 min^{-1} at 35 °C and 40 °C, respectively, asserting the effectiveness of elevated temperatures to bromate reduction kinetics using HPCO catalyzed $NaBH_4$. Additionally, as k_{obs} was increased along with higher temperatures, the relationship between k_{obs} and temperatures was further correlated via the Arrhenius equation as follows (Eq. (6)):

$$\ln k_{obs} = \ln A - E_a/RT \qquad (6)$$

where A represents the pre-exponential factor (min^{-1}); R is the gas constant (J/K mol); T is temperature of solution in Kelvin (K); E_a is the activation energy (kJ/mol). A plot (Fig. S7) indicated the correlation of Ln k_{obs} versus $1/T$, indicating that the data points were well-fitting by linear regression ($R^2 = 0.997$), then E_a was calculated as 28.5 kJ/mol. For comparisons, E_a values of the reported studies for bromate reduction were also summarized and listed in Table S3; and E_a of HPCO was considerably lower than many reported values by different catalysts, including

precious metal catalysts. This result confirms that HPCO is a robust and competitive heterogeneous catalyst for bromate reduction.

On the other hand, bromate removal efficiencies and bromide generation capacities were also presented in Fig. 8(b) and (c), respectively. One can be noted that the bromate removal efficiencies could be reached to the equilibrium faster as the increase of temperature. In particular, while bromate removal efficiency afforded to equilibrium state in 20 min at 30°C, it was even in a shorter time at higher temperatures (Fig. 8(b)). Besides, bromide generation capacities were also illustrated as shown in Fig. 8(c), indicating that bromide was also quickly produced when temperatures raised, which were corresponded to bromate reduction efficiencies. These results certainly certified the advantageous of elevated temperatures to bromate reduction using HPCO catalyzed $NaBH_4$.

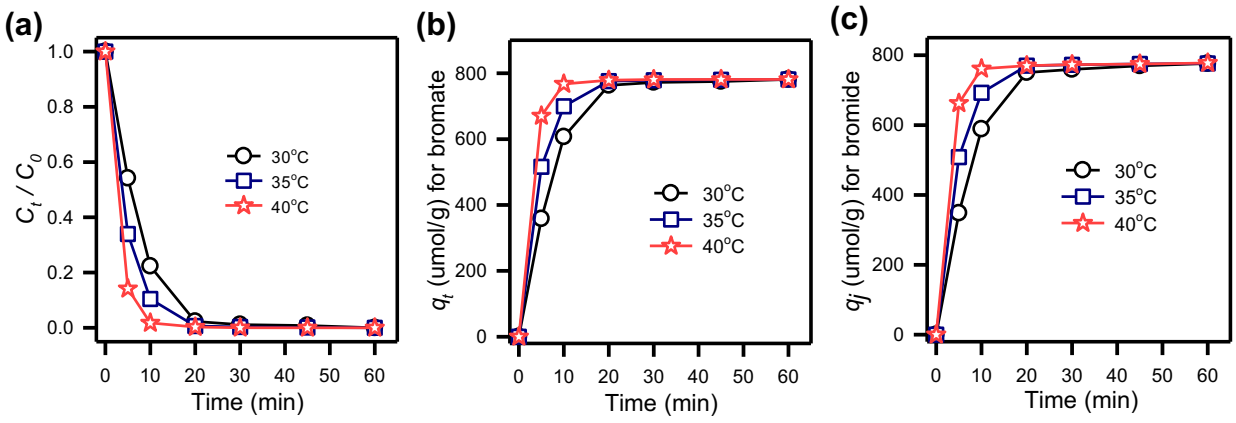

Fig. 8. Effect of temperatures on bromate reduction using HPCO+$NaBH_4$ (HPCO = 100 mg/L, $NaBH_4$ = 100 mg/L, T = 30°C).

3.5 Effect of initial pH of bromate solution

Since bromate reduction was performed using water batch experiments, pH of the solution is another crucial parameter affecting bromate reduction efficiency. Thus, the effect of different pH was further evaluated by adjusting the initial pH of bromate solution from 3 to 11. Fig. 9(a)

presents bromate reduction efficiency at various pH; and it can be noted that bromate reduction was slightly accelerated at lower pH of acidic conditions (i.e., pH = 3, 5) whereas bromate reduction was certainly influenced at higher pH of basic conditions (i.e., pH = 9, 11). In particular, at neutral condition of pH = 7, bromate was totally reduced within 20 min. When pH was lightly lowered as pH = 5, bromate was reduced faster, which could be even much faster at strongly acidic condition of pH = 3. In contrast, bromate was slowly reduced at slightly basic condition of pH =9 whereas it was even much influenced at strongly basic condition of pH =11. This demonstrates that bromate reduction was favorable in acidic conditions while higher pH of basic conditions seemed to be adverse for bromate reduction using HPCO catalyzed $NaBH_4$. The surface charges of HPCO were more positive at acidic conditions (as shown in zeta potentials analysis). Thus, anionic bromate ions were more attracted via electrostatic attraction force to the positive surface of HPCO where $NaBH_4$ was catalyzed to produce H_2 gas, thereby reducing bromate quickly [53]. Nevertheless, bromate reduction efficiencies were certainly decreased in basic conditions due to electrostatic repulsion between anionic bromate ions and more-negatively surface charges of HPCO, then leading to inefficient bromate reduction [53]. Moreover, bromate reduction efficiencies and bromide generation capacities at various pH values were also determined as displayed in Fig. 9(b) and (c), respectively. And one can be seen that lower pH was more beneficial for bromate reduction efficiencies and bromide generation capacities while higher pH was certainly unfavorable. However, bromate removal efficiencies and bromide generation capacities were still comparable at various pH values by using HPCO+$NaBH_4$ system.

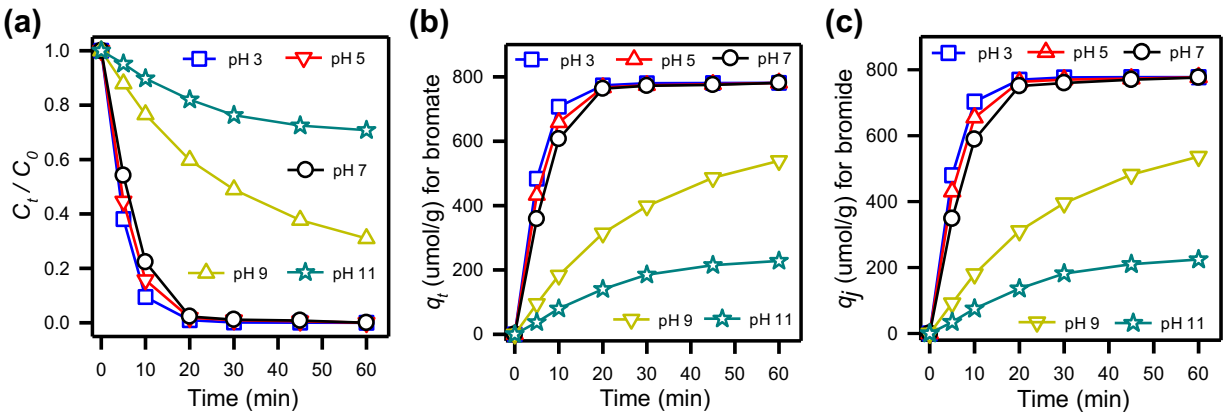

Fig. 9. Effect of pH on bromate reduction using HPCO+$NaBH_4$ (HPCO = 100 mg/L, $NaBH_4$ = 100 mg/L, T = 30°C).

3.6 Effect of co-existing anions on bromate reduction

Since bromate is usually found in water where consisted of many ions, especially anions, it is necessary to investigate the effect of co-existing anions (i.e., nitrate, sulfate, phosphate) to bromate reduction using HPCO catalyzed $NaBH_4$. Before evaluating the effect of different anions, bromate solution containing equivalent concentration (i.e., 10 mg/L) of those co-existing anions was firstly prepared. As shown in Fig. 10(a), bromate reduction was slightly slower in the presence of co-existing anions. However, 100% of bromate removal was still afforded after 60 min, revealing the superior catalytic activities of HPCO catalyzed $NaBH_4$ for bromate reduction, even in a complex matrix of various anions. Besides, the generation of bromide converted from bromate reduction was also necessarily quantified; and there was no significant difference of bromide generation with or without co-existing anions (Fig. 10(b)), proving that HPCO+$NaBH_4$ was still capable to reduce bromate to bromide in the presence of those competing anions. Interestingly, while the concentration of phosphate and sulfate were unchanged by HPCO catalyzed $NaBH_4$, a small amount of nitrate was certainly removed after 60 min as C_t/C_0 was 0.77. This result implies that

HPCO+$NaBH_4$ could also remove/reduce nitrate in water to produce nitrite, which is also reported in previous literature [11].

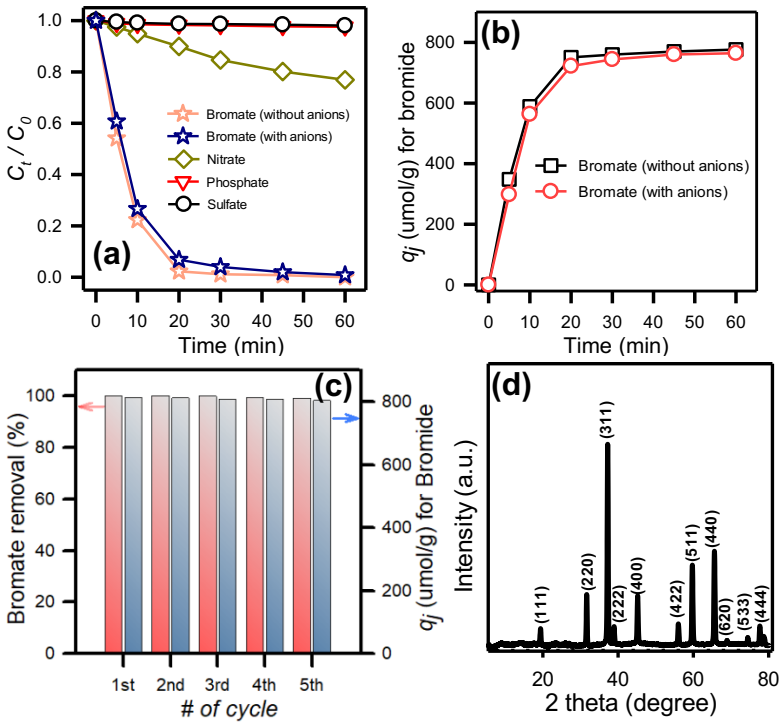

Fig. 10. Effect of co-existing anions on bromate reduction using HPCO+$NaBH_4$ (a) removal efficiency for bromate, and (b) conversion efficiency for bromide; (c) recyclability test of HPCO for bromate reduction (HPCO = 100 mg/L, $NaBH_4$ = 100 mg/L, T = 30°C), and (d) XRD pattern of used HPCO.

3.7 Recyclability of HPCO

Since HPCO showed superior catalytic activities for catalyzing $NaBH_4$ to reduce bromate in water, it is crucial to investigate the reusability of HPCO for continuous bromate reduction. As shown in Fig. 10(c), bromate removal efficiencies were almost unchanged as almost 100% bromate removal

was still afforded while the generation of bromide was also remained after five-consecutive cycles. Fig. 10 (d) reveals that the spent HPCO showed a very comparable XRD pattern to that of original HPCO without significant variations, indicating the high stability of HPCO over the multiple-cycle application. This result confirms that HPCO was highly reusable with outstanding-stable catalytic activities reduce bromate to bromide in water, even without any regeneration treatment.

4. Conclusion

In this study, a 2D hexagonal porous Co_3O_4 (HPCO) was successfully fabricated via one-step calcination of a coordinated framework CoTMC. The resulting HPCO not only retained the original 2D hexagonal morphology of the pristine CoTMC, but also comprised of many pores and Co_3O_4 NP distributing evenly over the surface. More importantly, this HPCO exhibited remarkable surficial oxygen vacancies as well as textural properties in comparison with the commercial Co_3O_4 NP. These significant characteristics of HPCO contributed to its outstanding catalytic activities for catalyzing $NaBH_4$ to reduce bromate in water. Moreover, HPCO also exhibited a low E_a of 28.5 kJ/mol for bromate reduction, which is lower than the reported values by many catalysts, especially noble metal catalysts. HPCO could also retain its high catalytic activities for bromate reduction and bromide generation over multiple-cycles, making it an outstanding and promising heterogeneous catalyst for bromate reduction via catalytic hydrogenation in water.

References:

1. Soltermann, F., et al., *Bromide Sources and Loads in Swiss Surface Waters and Their Relevance for Bromate Formation during Wastewater Ozonation.* Environmental Science & Technology, 2016. **50**(18): p. 9825-9834.

2. Garcia-Villanova, R.J., et al., *Occurrence of bromate, chlorite and chlorate in drinking waters disinfected with hypochlorite reagents. Tracing their origins.* Science of the Total Environment, 2010. **408**(12): p. 2616-2620.
3. Pinkernell, U. and U. von Gunten, *Bromate minimization during ozonation: Mechanistic considerations.* Environmental Science & Technology, 2001. **35**(12): p. 2525-2531.
4. von Gunten, U. and J. Hoigne, *Bromate Formation during Ozonization of Bromide-Containing Waters: Interaction of Ozone and Hydroxyl Radical Reactions.* Environ Sci Technol, 1994. **28**(7): p. 1234-42.
5. Liu, K., J.H. Lu, and Y.F. Ji, *Formation of brominated disinfection by-products and bromate in cobalt catalyzed peroxymonosulfate oxidation of phenol.* Water Research, 2015. **84**: p. 1-7.
6. Lin, K.Y.A. and S.Y. Chen, *Catalytic Reduction of Bromate Using ZIF-Derived Nanoscale Cobalt/Carbon Cages in the Presence of Sodium Borohydride.* Acs Sustainable Chemistry & Engineering, 2015. **3**(12): p. 3096-3103.
7. Listiarini, K., et al., *Hybrid coagulation-nanofiltration membrane for removal of bromate and humic acid in water.* Journal of Membrane Science, 2010. **365**(1-2): p. 154-159.
8. Bhatnagar, A., et al., *Bromate removal from water by granular ferric hydroxide (GFH).* Journal of Hazardous Materials, 2009. **170**(1): p. 134-140.
9. Zhong, Y., et al., *Denitrifying microbial community with the ability to bromate reduction in a rotating biofilm-electrode reactor.* Journal of Hazardous Materials, 2018. **342**: p. 150-157.
10. Chen, H., et al., *Aqueous bromate reduction by catalytic hydrogenation over Pd/Al2O3 catalysts.* Applied Catalysis B-Environmental, 2010. **96**(3-4): p. 307-313.
11. Lin, K.-Y.A., H.-A. Chang, and R.-C. Chen, *MOF-derived magnetic carbonaceous nanocomposite as a heterogeneous catalyst to activate oxone for decolorization of Rhodamine B in water.* Chemosphere, 2015. **130**: p. 66-72.
12. Restivo, J., et al., *Metal assessment for the catalytic reduction of bromate in water under hydrogen.* Chemical Engineering Journal, 2015. **263**: p. 119-126.
13. Lin, K.Y.A., et al., *Enhanced photocatalytic reduction of concentrated bromate in the presence of alcohols.* Chemical Engineering Journal, 2016. **303**: p. 596-603.
14. Chiu, Y.T., et al., *Reductive and adsorptive elimination of bromate from water using Ru/C, Pt/C and Pd/C in the absence of H-2: A comparative study.* Process Safety and Environmental Protection, 2019. **127**: p. 36-44.
15. Chiu, Y.T., et al., *Elimination of bromate from water using aluminum beverage cans via catalytic reduction and adsorption.* Journal of Colloid and Interface Science, 2018. **532**: p. 416-425.
16. Marco, Y., et al., *Bromate catalytic reduction in continuous mode using metal catalysts supported on monoliths coated with carbon nanofibers.* Chemical Engineering Journal, 2013. **230**: p. 605-611.
17. Pena-Alonso, R., et al., *A picoscale catalyst for hydrogen generation from NaBH4 for fuel cells.* Journal of Power Sources, 2007. **165**(1): p. 315-323.
18. Wei, Y.S., et al., *Fast hydrogen generation from NaBH4 hydrolysis catalyzed by nanostructured Co-Ni-B catalysts.* International Journal of Hydrogen Energy, 2017. **42**(9): p. 6072-6079.
19. Li, F., Q. Li, and H. Kim, *CoB/open-CNTs catalysts for hydrogen generation from alkaline NaBH4 solution.* Chemical Engineering Journal, 2012. **210**: p. 316-324.
20. Liu, B.H. and Z.P. Li, *A review: Hydrogen generation from borohydride hydrolysis reaction.* Journal of Power Sources, 2009. **187**(2): p. 527-534.

21. Nurlan, N., et al., *Enhanced reduction of aqueous bromate by catalytic hydrogenation using the Ni-based Metal-organic framework Ni(4,4'-bipy)(1,3,5-BTC) with NaBH4.* Chemical Engineering Journal, 2021. **414**: p. 128860.
22. Lin, K.Y.A. and S.Y. Chen, *Bromate reduction in water by catalytic hydrogenation using metal-organic frameworks and sodium borohydride.* Rsc Advances, 2015. **5**(54): p. 43885-43896.
23. Palomares, A.E., et al., *The use of Pd catalysts on carbon-based structured materials for the catalytic hydrogenation of bromates in different types of water.* Applied Catalysis B-Environmental, 2014. **146**: p. 186-191.
24. Restivo, J., et al., *Bimetallic activated carbon supported catalysts for the hydrogen reduction of bromate in water.* Catalysis Today, 2015. **249**: p. 213-219.
25. Chen, Y.J., et al., *Catalytic reduction of aqueous bromate by a non-noble metal catalyst of CoS2 hollow spheres in drinking water at room temperature.* Separation and Purification Technology, 2020. **251**.
26. Wu, Z., et al., *Reduction of bromate by zero valent iron (ZVI) enhances formation of brominated disinfection by-products during chlorination.* Chemosphere, 2021. **268**: p. 129340.
27. Lin, K.Y.A., C.H. Lin, and J.Y. Lin, *Efficient reductive elimination of bromate in water using zero-valent zinc prepared by acid-washing treatments.* Journal of Colloid and Interface Science, 2017. **504**: p. 397-403.
28. Tuan, D.D. and K.Y.A. Lin, *ZIF-67-derived Co3O4 rhombic dodecahedron as an efficient non-noble-metal catalyst for hydrogen generation from borohydride hydrolysis.* Journal of the Taiwan Institute of Chemical Engineers, 2018. **91**: p. 274-280.
29. Tuan, D.D., et al., *Porous hexagonal nanoplate cobalt oxide derived from a coordination polymer as an effective catalyst for activating Oxone in water.* Chemosphere, 2020. **261**.
30. Zhang, M., et al., *Promotion effects of halloysite nanotubes on catalytic activity of Co3O4 nanoparticles toward reduction of 4-nitrophenol and organic dyes.* Journal of Hazardous Materials, 2021. **403**.
31. Su, L.H., et al., *Electrochemical nitrate reduction by using a novel Co3O4/Ti cathode.* Water Research, 2017. **120**: p. 1-11.
32. Al Nafiey, A., et al., *Reduced graphene oxide decorated with Co3O4 nanoparticles (rGO-Co3O4) nanocomposite: A reusable catalyst for highly efficient reduction of 4-nitrophenol, and Cr(VI) and dye removal from aqueous solutions.* Chemical Engineering Journal, 2017. **322**: p. 375-384.
33. Keller, A.A., et al., *Stability and Aggregation of Metal Oxide Nanoparticles in Natural Aqueous Matrices.* Environmental Science & Technology, 2010. **44**(6): p. 1962-1967.
34. Tso, C.P., et al., *Stability of metal oxide nanoparticles in aqueous solutions.* Water Science and Technology, 2010. **61**(1): p. 127-133.
35. Zhu, J., et al., *Fast hydrogen generation from NaBH4 hydrolysis catalyzed by carbon aerogels supported cobalt nanoparticles.* International Journal of Hydrogen Energy, 2013. **38**(25): p. 10864-10870.
36. Tsai, Y.C., et al., *Metal organic framework-derived 3D nanostructured cobalt oxide as an effective catalyst for soot oxidation.* Journal of Colloid and Interface Science, 2020. **561**: p. 83-92.
37. Li, M.C., et al., *Cobalt-based coordination polymers as heterogeneous catalysts for activating Oxone to degrade organic contaminants in water: A comparative study.* Separation and Purification Technology, 2020. **236**.

38. Cheng, G.H., et al., *O-2(2-)/O- functionalized oxygen-deficient Co3O4 nanorods as high performance supercapacitor electrodes and electrocatalysts towards water splitting.* Nano Energy, 2017. **38**: p. 155-166.
39. Wang, D.W., Q.H. Wang, and T.M. Wang, *Morphology-Controllable Synthesis of Cobalt Oxalates and Their Conversion to Mesoporous Co3O4 Nanostructures for Application in Supercapacitors.* Inorganic Chemistry, 2011. **50**(14): p. 6482-6492.
40. Herrero, M., et al., *Nanosize cobalt oxide-containing catalysts obtained through microwave-assisted methods.* Catalysis Today, 2007. **128**(3): p. 129-137.
41. Patel, V.K., et al., *Combustion characterization and modeling of novel nanoenergetic composites of Co3O4/nAl.* Rsc Advances, 2015. **5**(28): p. 21471-21479.
42. Liu, Q., et al., *Dry citrate-precursor synthesized nanocrystalline cobalt oxide as highly active catalyst for total oxidation of propane.* Journal of Catalysis, 2009. **263**(1): p. 104-113.
43. Lou, Y., et al., *Promoting Effects of In2O3 on Co3O4 for CO Oxidation: Tuning O-2 Activation and CO Adsorption Strength Simultaneously.* Acs Catalysis, 2014. **4**(11): p. 4143-4152.
44. Li, L.D., et al., *Sub-10 nm rutile titanium dioxide nanoparticles for efficient visible-light-driven photocatalytic hydrogen production.* Nature Communications, 2015. **6**.
45. Naldoni, A., et al., *Effect of Nature and Location of Defects on Bandgap Narrowing in Black TiO2 Nanoparticles.* Journal of the American Chemical Society, 2012. **134**(18): p. 7600-7603.
46. Wang, Z., et al., *Surface oxygen vacancies on Co3O4 mediated catalytic formaldehyde oxidation at room temperature.* Catalysis Science & Technology, 2016. **6**(11): p. 3845-3853.
47. Feng, L.L., et al., *Metallic Co9S8 nanosheets grown on carbon cloth as efficient binder-free electrocatalysts for the hydrogen evolution reaction in neutral media.* Journal of Materials Chemistry A, 2016. **4**(18): p. 6860-6867.
48. Liu, L., et al., *Probing the Crystal Plane Effect of Co3O4 for Enhanced Electrocatalytic Performance toward Efficient Overall Water Splitting.* Acs Applied Materials & Interfaces, 2017. **9**(33): p. 27736-27744.
49. Wu, C., et al., *Cobalt boride catalysts for hydrogen generation from alkaline NaBH4 solution.* Materials Letters, 2005. **59**(14-15): p. 1748-1751.
50. Krishna, R., et al., *Novel synthesis of Ag@Co/RGO nanocomposite and its high catalytic activity towards hydrogenation of 4-nitrophenol to 4-aminophenol.* International Journal of Hydrogen Energy, 2015. **40**(14): p. 4996-5005.
51. Pandey, R.P., et al., *Reductive Sequestration of Toxic Bromate from Drinking Water using Lamellar Two-Dimensional Ti3C2TX (MXene).* Acs Sustainable Chemistry & Engineering, 2018. **6**(6): p. 7910-7917.
52. Zeino, A., et al., *Bromate Removal from Water Using Doped Iron Nanoparticles on Multiwalled Carbon Nanotubes (CNTS).* Journal of Nanomaterials, 2014. **2014**.
53. Wu, X.Q., et al., *Simultaneous Adsorption/Reduction of Bromate by Nanoscale Zerovalent Iron Supported on Modified Activated Carbon.* Industrial & Engineering Chemistry Research, 2013. **52**(35): p. 12574-12581.